Journal of Integrative Medicine xxx (xxxx) xxx

Contents lists available at ScienceDirect

Journal of Integrative Medicine

journal homepage: www.jcimjournal.com/jim
www.journals.elsevier.com/journal-of-integrative-medicine

Original Research Article

Honokiol protects against acute pancreatitis by activating SIRT3 to restore mitochondrial oxidative phosphorylation and alleviate hyperacetylation

Yi-fan Miao [a], Jia-qi Yao [b], Yang Peng [c], Ding Bai [d], Shu-han Fan [d], Hong-ying Li [d], Wei Jin [a], Yun Lu [a,*]

[a] Department of Emergency Medicine, Hospital of Chengdu University of Traditional Chinese Medicine, Chengdu 610072, Sichuan Province, China
[b] Department of Integrated Traditional Chinese and Western Medicine, West China Hospital of Sichuan University, Chengdu 610041, Sichuan Province, China
[c] School of Acupuncture and Tuina, Chengdu University of Traditional Chinese Medicine, Chengdu 611137, Sichuan Province, China
[d] School of Clinical Medicine, Chengdu University of Traditional Chinese Medicine, Chengdu 610072, Sichuan Province, China

ARTICLE INFO

Article history:
Received 22 November 2024
Accepted 17 December 2025
Available online xxxx

Keywords:
Acute pancreatitis
Honokiol
Sirtuin3
Oxidative phosphorylation
Cytochrome *c*1

ABSTRACT

Objective: Acute pancreatitis (AP) is a potentially life-threatening inflammatory disease with limited therapeutic options. Although honokiol has shown beneficial effects in animal models of AP, the mitochondrial mechanisms underlying these effects remain poorly understood. This study investigated whether honokiol protects against AP by activating the mitochondrial deacetylase sirtuin 3 (SIRT3) and regulating oxidative phosphorylation (OXPHOS) function.

Methods: A mouse model of caerulein-induced AP was established to assess the temporal expression of SIRT3 and the effects of its pharmacological inhibition. The efficacy of honokiol was evaluated in vivo using an AP mouse model and in vitro using 266-6 cells and primary pancreatic acinar cells. Proteomic analysis was performed to identify SIRT3-regulated mitochondrial proteins and pathways. Protein–protein docking and immunoprecipitation were used to validate the interaction and acetylation of the respiratory complex subunits.

Results: SIRT3 expression was markedly reduced in AP, while its inhibition exacerbated disease severity, confirming a protective role. Honokiol treatment restored SIRT3 expression, alleviated inflammation and mitochondrial damage, and partially rescued OXPHOS protein expression. The proteomic profiling identified three candidate OXPHOS subunits—adenosine triphosphate synthase membrane subunit K, cytochrome *c*1 (CYC1) and ubiquinol-cytochrome *c* reductase hinge protein—that were restored by honokiol treatment. The protein–protein docking analysis revealed strong binding affinity between SIRT3 and CYC1. The immunoprecipitation assay further confirmed that honokiol reduced the acetylation of CYC1, indicating that this effect is mediated by SIRT3 activity.

Conclusion: Honokiol activates SIRT3 and promotes deacetylation of the respiratory complex Ⅲ subunit CYC1, contributing to OXPHOS restoration and mitochondrial protection in AP. These findings suggest a previously unrecognized SIRT3–CYC1 signaling axis underlying honokiol's mitochondrial protective effects in AP.

Please cite this article as: Miao YF, Yao JQ, Peng Y, Bai D, Fan SH, Li HY, Jin W, Lu Y. Honokiol protects against acute pancreatitis by activating SIRT3 to restore mitochondrial oxidative phosphorylation and alleviate hyperacetylation. *J Integr Med*. 2026; Epub ahead of print.

1. Introduction

Acute pancreatitis (AP) represents a clinical emergency characterized by activation of digestive enzymes while they are still within the pancreatic acinar cells (PACs), leading to local necrosis and a systemic inflammatory response. Globally, the incidence of AP has risen steadily over the past six decades [1], with severe cases exhibiting mortality rates from 30% to 50% [2]. Current management remains largely supportive, including fluid resuscitation, analgesia and nutritional support [3], while targeted therapies such as protease inhibitors have shown limited efficacy due to poor

* Corresponding author.
E-mail address: 0550@cdutcm.edu.cn (Y. Lu).

https://doi.org/10.1016/j.joim.2026.01.007

specificity [4,5]. Emerging evidence suggests that mitochondrial dysfunction plays a central role in acinar cell injury [6]. Therefore, it is reasonable to infer that the limited efficacy of targeted therapies may stem from an insufficient understanding of mitochondrial contributions to AP pathogenesis—an area this study seeks to clarify.

The natural biphenolic compound honokiol, derived from Magnoliae Officinalis Cortex (the dried bark of *Magnolia officinalis* Rehder & E.H.Wilson), has emerged as a promising candidate for AP treatment. Previous studies have documented its protective effects that act through multiple mechanisms, including suppression of pro-inflammatory signaling pathways [7,8], modulation of metabolic profiles [9], and promotion of acinar cell apoptosis [10]. However, these effects remain largely phenotypic and lack integration into a unifying mitochondrial-related mechanism. This gap is particularly relevant because mitochondrial dysfunction is a key driver of AP pathogenesis [6]. Honokiol was initially identified as an activator of the oxidized form of nicotinamide adenine dinucleotide (NAD^+)-dependent protein deacetylase sirtuin 3 (SIRT3) in cardiovascular disease [11], highlighting its potential to modulate mitochondrial function through protein deacetylation. However, it is unclear whether honokiol exerts similar effects in AP and whether SIRT3 targets mitochondrial respiratory complexes as part of this response. This gap is further underscored by a recent study demonstrating that therapeutic fecal microbiota transplantation alleviates AP by increasing nicotinamide mononucleotide levels, which activate the SIRT3–peroxiredoxin 5 signaling pathway [12].

SIRT3, a predominant mitochondrial deacetylase, regulates cellular metabolism under stress by targeting proteins such as superoxide dismutase 2 [13,14]. While its antioxidant function has been partially explored in AP [12,13], its role in regulating mitochondrial respiration remains poorly understood. A recent study revealed that oxidative phosphorylation (OXPHOS) pathways were markedly disrupted during the progress of AP [15]. Notably, cytochrome *c*1 (CYC1), a core component of mitochondrial complex Ⅲ, was identified as a candidate regulator because electron transport efficiency could be influenced by acetylation of its binding partners [16]. Specifically, acetylation of cytochrome *c*, the electron acceptor for CYC1, was shown to impair electron transfer to complex Ⅳ [17], raising the possibility that CYC1 function is also acetylation-sensitive. This led us to hypothesize that SIRT3 may regulate the acetylation status of CYC1 as AP develops, potentially linking mitochondrial deacetylation to OXPHOS preservation. Therefore, this study investigated whether honokiol exerts its protective effects in AP through a SIRT3-mediated deacetylation mechanism that regulates mitochondrial OXPHOS. Particular attention was given to CYC1, a complex Ⅲ subunit whose involvement in AP has not been previously characterized.

2. Material and methods

2.1. Compounds and reagents

Honokiol (purity: 99.76%; HY-N0003) and 3-(1H-1,2,3-triazol-4-yl) pyridine (3-TYP, purity: 99.96%; HY-108331) were from MedChemExpress (Shanghai, China). Caerulein (purity ≥ 95%; S62702) was from Shanghai Yuanye Bio-Technology (Shanghai, China). Taurocholic acid sodium salt hydrate (NaT, purity ≥ 95%; T4009) and taurolithocholic acid 3-sulfate disodium salt (TLCS, purity ≥ 90%; T0512) were from Sigma–Aldrich (St. Louis, MO, USA).

2.2. Ethics and animals

All animal experiments were approved by the Institutional Animal Care and Use Committees of Chengdu University of Traditional Chinese Medicine (approval No. 2025012). Male C57BL/6 mice (8–10 weeks of age) were purchased from the Laboratory Animal Center of Sichuan University (certificate No. SCXK[川]2024-0026; Chengdu, Sichuan Province, China) and housed in a specific pathogen-free facility under standard conditions.

2.3. AP model and drug administration

Experimental AP was induced using a well-established protocol [18]. Mice received seven intraperitoneal (i.p.) injections of caerulein (50 μg/kg body weight, dissolved in sterile 0.9% saline) at 1-hour intervals. The mice in the control group received an equal volume of saline. This caerulein-induced AP model is widely used to mimic mild to moderate AP in mice [19]. For time-course analysis, mice were euthanized at 7, 12, 24 or 48 h after the first caerulein injection via cervical dislocation without anesthesia, in accordance with institutional ethical guidelines.

To evaluate pharmacological interventions, the SIRT3 inhibitor 3-TYP (50 mg/kg body weight, i.p.) was used. The compound was first dissolved in dimethyl sulfoxide (DMSO, 100 mg/mL), then diluted 1:20 in saline to a final concentration of 5 mg/mL. Mice received 3-TYP (200 μL per dose, i.p.) twice: 1 h before and 1 h after the first caerulein injection [20]. For honokiol treatment, the compound was prepared similarly: the compound was dissolved in DMSO at 100 mg/mL and diluted in saline to a final concentration of 0.5, 1 or 2 mg/mL. Mice received honokiol (200 μL per dose, via intragastric gavage) 1 h before the first caerulein injection, corresponding to 2.5, 5 or 10 mg/kg body weight [10]. In the rescue experiment, mice were pre-treated with honokiol (5 mg/kg body weight, via intragastric gavage) 1 h before their first caerulein injection, and co-treated with 3-TYP (50 mg/kg body weight, i.p.) 1 h before and 1 h after their first caerulein injection. Drug preparation and administration followed the same protocols as described above. All vehicle-treated animals received an equal volume of the diluted DMSO-saline solution.

Unless otherwise specified, blood and pancreatic tissue samples were collected 12 h after the first caerulein injection for downstream analyses. Sample sizes were determined based on prior laboratory experience, and preliminary experiments to ensure adequate statistical power while minimizing animal use [18].

2.4. Histopathology

Analysis of histopathology was performed as follows: after euthanasia, individual pancreas fragments were immediately collected, fixed in 10% formalin, embedded in paraffin, sectioned into 5 μm-thick slices, and stained with hematoxylin and eosin. The staining was performed by the laboratory of Servicebio Technology (Wuhan, Hubei Province, China). The stained slides were scanned using a Panoramic MIDI digital scanner (3DHISTECH, Budapest, Hungary). Pancreatic histopathology was evaluated by a professional pathologist in a blinded manner according to the Schmidt pathology scoring criteria, which includes edema, inflammation and necrosis (scores 0–3) [21].

2.5. Haematology

Initially, 50 μL of serum was diluted in 5× phosphate-buffered saline (PBS) solution. Pancreatic digestive enzyme parameters including serum amylase and lipase concentrations were detected using a cobas® 6000 c501 automatic biochemical analyzer (Roche Diagnostic, Basel, Switzerland) according to the manufacture's protocols.

2.6. Western blotting and immunoprecipitation

Western blotting and immunoprecipitation were carried out according to the procedures reported by Kang et al. [22]. Briefly, pancreatic tissues and acinar cells were lysed in radioimmunoprecipitation assay (RIPA) buffer (P0013, Beyotime Biotechnology, Shanghai, China) containing protease and phosphatase inhibitors, followed by homogenization or sonication as appropriate. For phosphorylation assays, extra protease and phosphatase inhibitor cocktail (P1045, Beyotime Biotechnology, Shanghai, China) was added. Total protein was determined using the Pierce™ 660 nm Protein Assay Reagent (22660, Thermo Scientific, Rockford, IL, USA), and proteins were separated using sodium dodecyl sulphate electrophoresis–polyacrylamide gel electrophoresis and transferred to nitrocellulose membranes. The separated proteins were detected using primary antibodies listed in Table 1.

For immunoprecipitation, pancreatic tissue lysates were prepared using a mild RIPA buffer (P0013D, Beyotime Biotechnology, Shanghai, China). Protein A/G magnetic beads (HY-K0202, MedChemExpress, Shanghai, China) were first incubated with 6 μg of anti-acetyllysine antibody for 30 min at room temperature on a rocking platform. The antibody-conjugated beads were then washed once with washing buffer (PBS containing 0.02% Triton X-100) for 5 min. Subsequently, 1 mL protein lysate (total protein concentration: 1 mg/mL) was added and incubated with the beads for an additional 30 min at room temperature. After incubation, the immunocomplexes were washed three times with washing buffer, eluted in Laemmli sample buffer, and denatured by boiling at 100 °C for 15 min. CYC1 was detected by Western blotting. The band intensity was quantified using Fiji (version 2.16.0) for densitometric analysis [23].

2.7. RNA extraction and quantitative real-time reverse transcription-polymerase chain reaction

Total RNA was routinely extracted from 15 mg of pancreatic tissue using E.Z.N.A.® total RNA kit I (R6834, Omega Bio-Tek, Norcross, GA, USA) and quantified using NanoDrop™ One/One^C (Thermo Scientific, Waltham, MA, USA). Then, 1 mg RNA sample was reversely transcribed into cDNA using the PrimeScript™ RT reagent kit with gDNA eraser (perfect real time) (RR047Q, Takara, Shiga, Japan). The polymerase chain reaction (PCR) amplification was performed with QuantStudio™ 6 Flex (Applied Biosystems, Carlsbad, CA, USA) using the TB Green® Premix Ex Taq™ II FAST qPCR (CN830A, Takara, Shiga, Japan) with specific primers (Table 2).

2.8. NAD^+ content assay in pancreatic tissues

Pancreatic tissue (20 mg) was homogenized in 200 μL of NAD^+ extraction buffer and processed according to the instructions provided with the CheKine™ micro coenzyme Ⅰ NAD(H) assay kit (KTB1020, Abbkine, Wuhan, Hubei Province, China). Absorbance was measured at 450 nm using an Infinite® 200 PRO microplate reader (Tecan, Männedorf, Switzerland). The NAD^+ content was normalized to total protein concentration in each sample.

2.9. Transmission electron microscopy

Pancreatic tissue samples (1 mm^3) were fixed in 2.5% glutaraldehyde at 4 °C overnight, rinsed with PBS, and post-fixed with 1% osmium tetroxide. After graded ethanol dehydration, the tissues were embedded in epoxy resin. Ultrathin sections were cut, double-stained with uranyl acetate and lead citrate, and imaged using a JEM-1400Flash transmission electron microscope (JEOL, Tokyo, Japan). At least three copper grids were prepared per sample, and representative regions were selected for imaging under low (10,000×) and high (25,000×) magnification, respectively.

2.10. Cell culture, cell viability and adenosine triphosphate quantification

The 266-6 cells (WN-10438, Warner Bio, Wuhan, Hubei Province, China) were cultured (37 ℃, 95% humidity and 5% CO_2) in Dulbecco's modified Eagle medium (L110KJ, BasalMedia Technologies, Shanghai, China) supplemented with 10% fetal bovine serum (10099141C, Thermo Scientific, Auckland, New Zealand) and 1% penicillin and streptomycin (BC-CE-007, Biochannel, Nanjing, Jiangsu Province, China). The identity of the cell line was confirmed through short tandem repeat profiling, and routine testing showed no mycoplasma contamination. After subculture and detachment, the cells were seed into 96-well plates at a density of 4×10^5-cells/mL. The cells were treated with honokiol (1.25, 2.5, 5, 10, 20, 40 and 80 μmol/L) for 12 h or NaT (2.5, 5, 10 and 20 mmol/L) for 1 h, and then cell viability was determined using cell counting kit-8 (C0037, Beyotime Biotechnology, Shanghai, China) according to the manufacturer's instructions. For adenosine triphosphate (ATP) detection, 266-6 cells were treated with 10 mmol/L NaT for 1 h, with or without a 12-hour pretreatment with 10 μmol/L honokiol. The control group received equal volumes of DMSO and PBS. Total ATP levels were measured using an ATP assay kit (S0026, Beyotime Biotechnology, Shanghai, China) according to the manufacturer's instructions.

2.11. PAC isolation, treatment and cytokine analysis

Primary PACs were isolated from C57BL/6 mice via collagenase Ⅳ (C9407, Sigma–Aldrich, St. Louis, MO, USA) digestion, filtered through a 100 μm cell strainer, and cultured at 37 °C in a humidified incubator. After centrifugation and washing, cells were resuspended in 4-(2-hydroxyethyl)-1-piperazineethanesulfonic acid-buffered saline. For stimulation, PACs were pretreated with honokiol (5 or 10 μmol/L) for 30 min. This was followed by co-incubation with TLCS (500 μmol/L) for an additional 30 min. Culture supernatants in pancreatic tissue were collected and analyzed for inflammatory cytokines using commercial enzyme-

Table 1
Primary antibodies used in WB analysis.

Antibody	Source	Identifier	Dilution
Anti-acetyllysine rabbit monoclonal antibody	PTM BIO (Hangzhou, Zhejiang Province, China)	PTM-105RM	1:1000
Anti-β-actin rabbit monoclonal antibody	ABclonal (Wuhan, Hubei Province, China)	#3195	1:10,000
Anti-CYC1 polyclonal antibody	Proteintech (Wuhan, Hubei Province, China)	10242-1-AP	1:1000
Anti-NF-κB p65 polyclonal antibody	Proteintech	10745-1-AP	1:1000
Anti-p-NF-κB p65 (Ser468) recombinant monoclonal antibody	Proteintech	82335-1-RR	1:3000
Total OXPHOS rodent WB antibody cocktail	Abcam (Cambridge, UK)	ab110413	1:1000
Anti-SIRT3 polyclonal antibody	Proteintech	10099-1-AP	1:1000

CYC1: cytochrome *c*1; NF-κB: nuclear factor-κB; OXPHOS: oxidative phosphorylation; p-NF-κB: phosphorylated NF-κB; SIRT3: sirtuin 3; WB: Western blotting.

Table 2
Primer sequences.

Gene	Forward sequence (5′→3′)	Reverse sequence (5′→3′)	Size (bp)
Tnf	ACGGCATGGATCTCAAAGACA	GTGAGGAGCACGTAGTCGG	112
Il1b	GAAATGCCACCTTTTGACAGTGAT	TTCTCCACAGCCACAATGAGT	188
Actb	CAGGTCATCACTATTGGCAAC	TCTTTACGGATGTCAACGTCA	140

Actb: actin β; *Il1b*: interleukin 1β; *Tnf*: tumor necrosis factor.

linked immunosorbent assay (ELISA) kits: mouse tumor necrosis factor-α (TNF-α) ELISA kit (EM0183), interleukin-1β (IL-1β) ELISA kit (EM0109) and IL-6 ELISA kit (EM0121), according to the manufacturer's instructions (Wuhan Feyen Biotechnology, Wuhan, Hubei Province, China). Cytokine concentrations were calculated from standard curves.

2.12. Hoechst 33342/propidium iodide staining

The 266-6 cells were seeded in 24-well plates at a density of 2×10^5 cells/mL, and then treated with 10 m mol/L NaT for 6 h, with or without a 12-hour pretreatment with 10 μmol/L honokiol. PACs were processed similarly, as described in the Section 2.11. The Hoechst 33342/propidium iodide (PI) double-staining kit (CA1120, Solarbio, Beijing, China) was used to evaluate cell death. After staining, the cells were washed with PBS and visualized under an IX83 epifluorescence microscope (Olympus, Tokyo, Japan). The proportion of necrotic cells was quantified by calculating the ratio of PI-positive nuclei (indicating membrane integrity loss) to Hoechst 33342-stained nuclei (total) using Fiji software.

2.13. Imaging of dihydroethidium fluorescence

The 266-6 cells were seeded into 24-well plates at a density of 2×10^5 cells/mL, and then treated with 5 mmol/L NaT for 6 h, with or without a 12-hour pretreatment with 10 μmol/L honokiol. The production of oxidative stress/reactive oxygen species (ROS) was assessed by dihydroethidium (DHE; 50102ES02, Yeasen Biotechnology, Shanghai, China) fluorescence. Briefly, cells were incubated with 5 μmol/L DHE for 30 min, followed by imaging and fluorescence intensity analysis using an IX83 epifluorescence microscope and a Celigo™ 200-BFFL-5C imaging cytometer (Nexcelom Bioscience, Lawrence, MA, USA), respectively. All experimental procedures were carried out at room temperature.

2.14. Quantitative proteomics and bioinformatic analysis

Pancreas tissue was homogenized in liquid nitrogen and extracted with lysis buffer containing 1% sodium dodecyl sulfate and 1% protease inhibitor. The protein solution was reduced with 5 mmol/L dithiothreitol for 30 min at 56 °C, alkylated with 11 mmol/L iodoacetamide for 15 min at room temperature in the dark, and then diluted with 200 mmol/L triethylammonium bicarbonate to achieve a urea concentration below 2 mol/L. Trypsin was then added at a trypsin-to-protein mass ratio of 1:50 for overnight digestion, followed by a second digestion at a ratio of 1:100 for 4 h. The peptides were desalted using a Strata-X 33 μm polymeric reversed phase extraction column (8B-S100-AAK, Phenomenex, Torrance, CA, USA). For liquid chromatography–tandem mass spectrometry, peptides were separated on an EASY-nLC™ 1200 ultra-performance liquid chromatography system and analyzed with an Orbitrap Exploris™ 480 mass spectrometer (Thermo Scientific, Waltham, MA, USA). Data-independent acquisition (DIA) data were processed using DIA-NN (version 1.8, Demichev, Ralser and Lilley labs, University of Cambridge, Cambridge, UK) [24], and tandem mass spectra were searched against the Swiss-Prot database of *Mus musculus* (17,132 entries) with a reverse decoy database. Trypsin/P was set as the cleavage enzyme, allowing for one missed cleavage, with fixed modifications of N-terminal methionine excision and cysteine carbamidomethylation. The false discovery rate was set to < 1%.

Unless otherwise specified, all visualizations in the following analyses were generated using the PTMCloud tool (PTM BIO, Hangzhou, Zhejiang Province, China; https://www.ptm-biolab-css.com.cn/cloudIndex). Principal component analysis (PCA) was used to assess the quantitative consistency of biological or technical replicate samples. The relative quantitative values of all samples were used to generate a PCA plot. A Student's *t*-test was used to assess differences in protein abundance. Differentially expressed proteins (DEPs) were identified as those with a fold change > 1.3 (upregulated) or < 1/1.3 (downregulated) and $P < 0.05$. DEPs were visualized through volcano plots. MitoCarta3.0 (Broad Institute, Cambridge, MA, USA) was used to identify the sub-mitochondrial locations and biochemical pathways of DEPs [25]. OXPHOS proteins were visualized using a heatmap. Afterwards, protein–protein interactions (PPIs) were analyzed on the Search Tool for the Retrieval of Interacting Genes/Proteins (STRING) database (https://string-db.org) with a required minimum interaction score > 0.7 and visualized with Cytoscape (version 3.9.1, Cytoscape Consortium, San Diego, CA, USA) [26]. Additionally, Gene Set Enrichment Analysis (GSEA) was performed using the mouse hallmark gene sets from the Molecular Signatures Database (MSigDB) collections (v2022.1) [27,28].

2.15. Molecular docking

The molecular structure of honokiol was obtained from the PubChem database (https://pubchem.ncbi.nlm.nih.gov/). The 3D structures of proteins were downloaded from the Protein Data Bank (https://www.rcsb.org/) and AlphaFold (https://alphafold.com/). The water molecules were excluded, polar hydrogen atoms were added, charges for the protein were calculated, and rotatable bonds for the molecular ligand were detected. Both structures were then saved in the pdbqt format. Molecular docking calculations were carried out using the AutoDock (version 4.2) and AutoDockTools (version 1.5.7, The Scripps Research Institute, La Jolla, CA, USA) [29]. Data were visualized using PyMOL (version 2.4.0, Schrödinger, New York, NY, USA).

2.16. Statistical analysis

GraphPad Prism 8.0 (GraphPad Software, San Diego, CA, USA) was used for statistical analysis. Data are presented as mean ± standard error of the mean, unless otherwise specified. The normality of data distributions was assessed using the Shapiro–Wilk test. For normally distributed data, comparisons between two groups were performed using Student's *t*-test (or Welch's correction for unequal variances), and comparisons among multiple groups were performed using one-way analysis of variance. For non-normally distributed data, the Kruskal–Wallis test was applied. When multiple groups were compared, Dunn's multiple comparisons test was used as a post hoc test. A *P* value < 0.05 was considered statistically significant.

3. Results

3.1. Severity of AP correlates with reduced pancreatic SIRT3 expression and is exacerbated by SIRT3 inhibition

To characterize the progression of AP, we first established a caerulein-induced AP model and collected pancreatic tissue at 0, 7, 12, 24 and 48 h after the initial injection. As shown in Fig. 1A, acinar cell necrosis and histological scores markedly increased by 7 h and peaked at 12 h post-injection. Serum amylase and lipase levels exhibited a similar trend (Fig. 1B). Meanwhile, SIRT3 expression progressively decreased and reached its lowest level at 12 h (Fig. 1C). Based on these findings, 12 h post-caerulein induction was selected as the optimal time point for subsequent experiments.

SIRT3 reduction was accompanied by increased global protein acetylation in the pancreas (Fig. 1D), as well as elevated mRNA levels of pro-inflammatory cytokines tumor necrosis factor (*Tnf*) and interleukin 1β (*Il1b*) (Fig. 1E). To assess the functional relevance of SIRT3 downregulation, we used 3-TYP, a pharmacological inhibitor with high selectivity for SIRT3 over other sirtuin isoforms (Fig. 1F) [30]. The administration of 3-TYP significantly worsened pancreatic injury, as evidenced by increased histological scores and elevated serum amylase and lipase (Figs. 1G and 1H). Moreover, 3-TYP treatment led to a higher degree of protein acetylation compared to the AP model group (Fig. 1I), supporting a protective role for SIRT3 through the regulation of protein acetylation during AP progression.

3.2. Honokiol reduces pancreatic injury and hyperacetylation in AP through SIRT3-associated mechanisms

To explore the role of SIRT3 in the protective effect of honokiol against AP, we examined its binding affinity with the SIRT3 protein via molecular docking, which revealed a binding energy of –6.6 kcal/mol (Fig. 2A), consistent with previous reports describing honokiol as a SIRT3 activator [11]. The workflow of further experimental validation is illustrated in Fig. 2B. Representative images of freshly harvested pancreatic tissue from each group are presented in Fig. 2C. Mice were pretreated with honokiol at different doses (2.5, 5 or 10 mg/kg) prior to caerulein injection. Histological analysis showed that honokiol significantly reduced pancreatic injury induced by caerulein, with all three doses resulting in lower histological scores ($P < 0.05$, Fig. 2D). In parallel, serum amylase and lipase levels were markedly decreased after treatment with honokiol at 5 and 10 mg/kg ($P < 0.001$, Fig. 2E). As the protective effects of honokiol of two doses were comparable, 5 mg/kg was selected for subsequent experiments. Honokiol pretreatment notably restored SIRT3 expression ($P = 0.0161$, Fig. 2F) and attenuated global protein acetylation in pancreatic tissue ($P < 0.05$, Fig. 2G). In addition, the level of phosphorylated p65 (p-p65), a marker of nuclear factor-κB (NF-κB) pathway activation, was significantly increased in AP mice ($P = 0.034$), which was suppressed by honokiol ($P = 0.0172$, Fig. 2F). Correspondingly, the mRNA levels of inflammatory cytokines *Tnf* and *Il1b* were also reduced in honokiol-treated mice (Fig. 2H), suggesting that honokiol alleviates pancreatic inflammation potentially through modulation of SIRT3 activity and acetylation-related signaling.

3.3. SIRT3 inhibition reverses the protective effects of honokiol in AP

To assess whether the effects of honokiol depend on SIRT3 activity, a rescue experiment was performed by co-administering the selective SIRT3 inhibitor 3-TYP (Fig. 3A). Compared with monotherapy with honokiol, co-treatment with 3-TYP partially reversed the protective effects of honokiol on serum amylase and lipase levels and pancreatic injury (Figs. 3B and 3C). While SIRT3 protein expression remained unchanged, 3-TYP treatment partially reversed honokiol-induced suppression of p-p65 and restoration of pan-acetylated proteins (Figs. 3D and 3E), indicating that SIRT3 enzymatic activity is required for the protective effect. Compared with the control group, AP mice exhibited a significant reduction in pancreatic NAD^+ level ($P = 0.0003$, Fig. 3F) and SIRT3 expression ($P < 0.0001$, Fig. 3D), suggesting that NAD^+ depletion may contribute to SIRT3 suppression during disease onset. The administration of honokiol modestly increased NAD^+ level, which, however, was not statistically significant. Compared to the honokiol monotherapy, the co-administration with 3-TYP further reduced NAD^+ ($P = 0.0013$, Fig. 3F), implying a potential feedback relationship between NAD^+ availability and SIRT3 activity.

3.4. Proteomic analysis reveals impaired mitochondrial OXPHOS in AP

To investigate mitochondrial involvement in caerulein-induced AP, quantitative proteomic analysis was performed on pancreatic tissue samples from control and AP mice. A total of 39,669 peptides and 6582 proteins were quantified. PCA showed a clear separation between the two groups (Fig. 4A), and differential expression analysis identified 1070 DEPs, with 774 upregulated and 296 downregulated in the caerulein-induced AP (Fig. 4B). To examine mitochondrial changes specifically, we cross-referenced the DEPs with the MitoCarta 3.0 database, which contains 1140 mitochondrial proteins in mice, identifying 79 mitochondria-associated DEPs. Submitochondrial compartment analysis revealed that these proteins were predominantly localized to the mitochondrial matrix (41.77%) and inner membrane (29.11%, Fig. 4C). Functional enrichment analysis indicated that OXPHOS was the most significantly enriched mitochondrial pathways following metabolic processes (Fig. 4D). A heatmap of OXPHOS-related DEPs showed that 14 of 16 proteins were downregulated in AP tissues (Fig. 4E). PPI network analysis of 79 mitochondrial DEPs revealed prominent clusters involving OXPHOS components and mitochondrial transcription/translation-related proteins (Fig. 4F), including a total of nine OXPHOS-related proteins most closely associated with AP pathology. Given that mitochondrial DEPs constituted only 7.38% of all DEPs, we performed GSEA independent of DEP filtering, which confirmed significant downregulation of the OXPHOS pathway in AP samples (Fig. 4G).

3.5. Honokiol restores mitochondrial structure and OXPHOS protein expression in AP

To validate the proteomic findings of mitochondrial OXPHOS disruption in caerulein-induced AP, we further examined mitochondrial ultrastructure and OXPHOS protein levels in the rescue experimental setting. Transmission electron microscopy showed well-preserved mitochondrial morphology in the control group, whereas samples of pancreatic tissue from AP mice showed evident structural damage, including swollen mitochondria and cristae fragmentation (Fig. 5A). Honokiol pretreatment partially preserved mitochondrial integrity, while co-administration of 3-TYP reversed this protective effect. Western blotting analysis using a multiplex OXPHOS antibody cocktail revealed that, compared with the control group, AP mice exhibited significant downregulation of most representative OXPHOS complex subunits, including ATP synthase F1 subunit α (ATP5F1A, complex Ⅴ; $P = 0.0273$), ubiquinol-cytochrome *c* reductase core protein 2 (UQCRC2, complex Ⅲ; $P = 0.0474$), and mitochondrially encoded cytochrome *c* oxidase Ⅰ (MT-CO1,

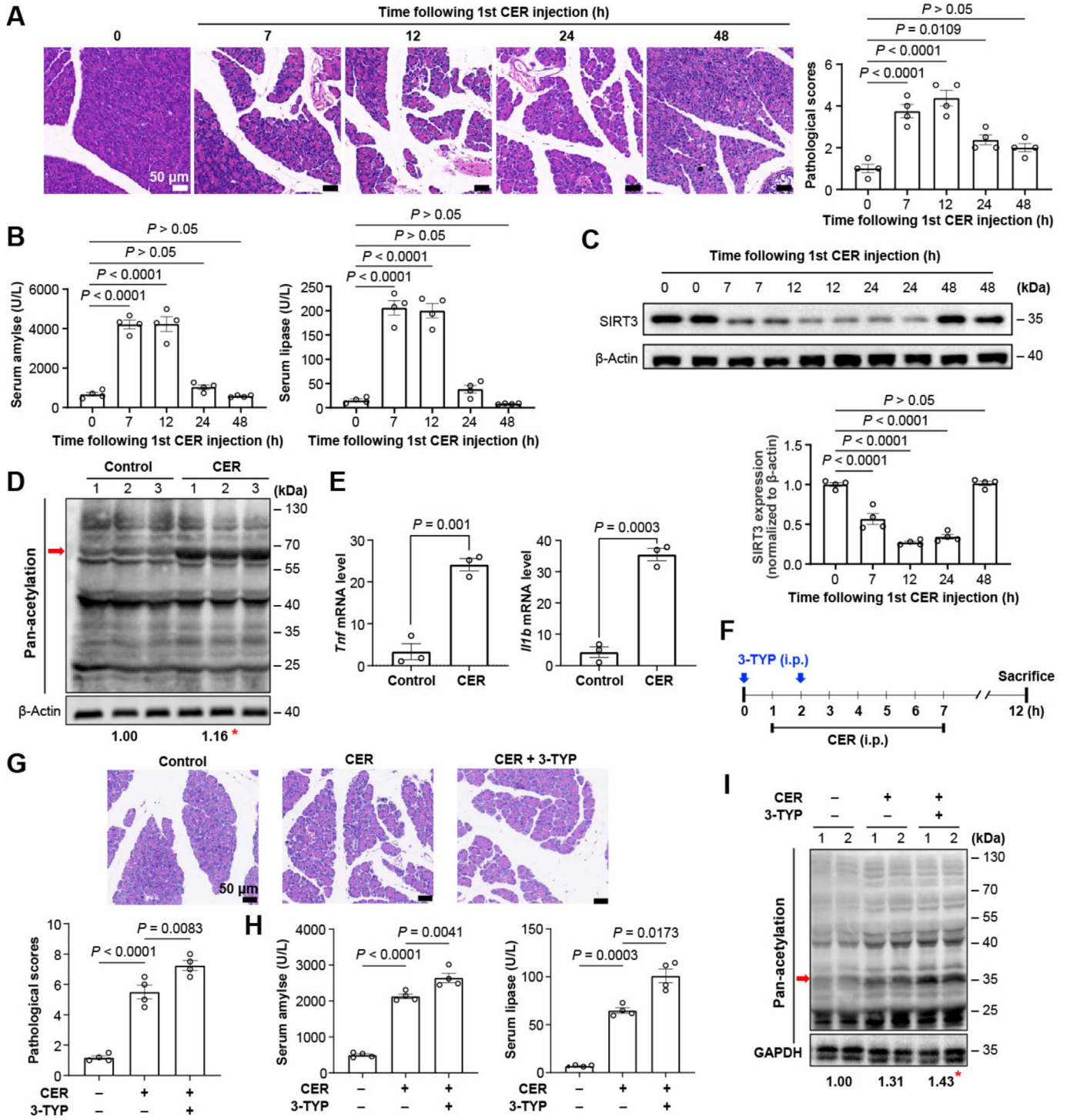

Fig. 1. Severity of acute pancreatitis correlates with reduced pancreatic SIRT3 expression and is exacerbated by SIRT3 inhibition. **A:** Representative images of H&E-stained pancreatic tissues at different time points after CER injection (magnification: 200×) and quantitative analysis of pathological scores (n = 4). **B:** Serum amylase and lipase levels (n = 4). **C:** Representative images of Western blot analysis of SIRT3 expression across time points in pancreatic tissues and quantitative analysis of protein levels (n = 4). **D:** Western blotting analysis of pan-acetylated proteins in pancreatic tissues (n = 3). **E:** Relative mRNA levels of *Tnf* and *Il1b* in pancreatic tissues (n = 3). **F:** Schematic illustration of 3-TYP administration in the SIRT3 inhibition experiment. **G:** H&E-stained pancreatic sections following 3-TYP administration (magnification: 200×) and quantitative analysis of pathological scores (n = 4). **H:** Serum amylase and lipase levels following 3-TYP administration (n = 4). **I:** Western blotting analysis of pan-acetylated proteins following 3-TYP administration in pancreatic tissues (n = 2). Data are expressed as mean ± standard error of mean. $^*P < 0.05$, *vs* control group. 3-TYP: 3-(1H-1,2,3-triazol-4-yl) pyridine; CER: caerulein; GAPDH: glyceraldehyde-3-phosphate dehydrogenase; H&E: hematoxylin and eosin; *Il1b*: interleukin 1β; i.p.: intraperitoneal; SIRT3: sirtuin 3; *Tnf*: tumor necrosis factor.

complex Ⅳ; P = 0.0172). The expression of NADH:ubiquinone oxidoreductase subunit B8 (NDUFB8, complex Ⅰ) also showed a trend of downregulation (P = 0.0633), while expression of succinate dehydrogenase complex iron sulfur subunit B (SDHB, complex Ⅱ) remained unchanged (Fig. 5B). The treatment with honokiol significantly restored the levels of ATP5F1A (P = 0.0268), UQCRC2 (P = 0.0271) and MT-CO1 (P = 0.017), compared to the AP group. Although co-treatment with 3-TYP

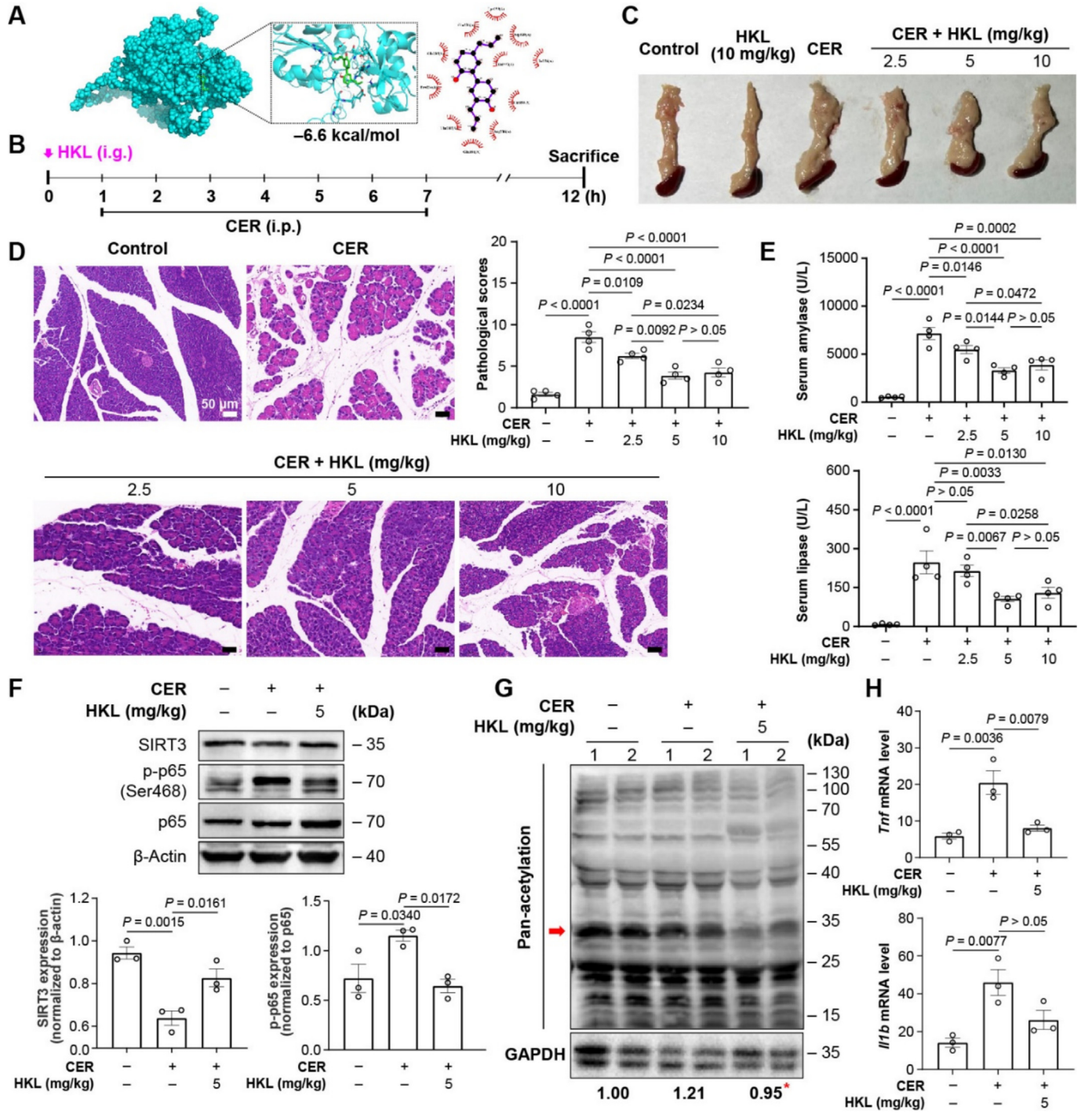

Fig. 2. HKL reduces pancreatic injury and hyperacetylation in AP through SIRT3-associated mechanisms. **A:** Molecular docking model showing the interaction between HKL and SIRT3. **B:** Schematic illustration of HKL administration in the CER-induced AP model. **C:** Representative images of freshly harvested pancreatic tissues. **D:** Pancreatic sections stained with hematoxylin and eosin (magnification: 200×) and quantitative analysis of pathological scores (n = 4). **E:** Serum amylase and lipase levels (n = 4). **F:** Representative images of Western blotting analysis of SIRT3, p65 and p-p65 in pancreatic tissues and quantitative analysis of protein levels (n = 3). **G:** Representative images of Western blotting analysis of pan-acetylated proteins in pancreatic tissues (n = 2). **H:** Relative mRNA levels of *Tnf* and *Il1b* in pancreatic tissues (n = 3). Data are expressed as mean ± standard error of mean. *P < 0.05, *vs* control group. AP: acute pancreatitis; CER: caerulein; GAPDH: glyceraldehyde-3-phosphate dehydrogenase; HKL: honokiol; *Il1b*: interleukin 1β; i.g.: intragastric gavage; i.p.: intraperitoneal; p65: nuclear factor-κB p65; p-p65: phosphorylated p65; SIRT3: sirtuin 3; *Tnf*: tumor necrosis factor.

mildly suppressed these restorative effects, the differences were not statistically significant. These findings corroborate the proteomic data and suggest that honokiol mitigates mitochondrial damage in AP, potentially via SIRT3-mediated stabilization of OXPHOS subunits.

3.6. Honokiol reduces NaT-induced oxidative stress, necrosis and inflammation in 266-6 cells

To evaluate the effects of honokiol in vitro, we tested its cytotoxicity in pancreatic acinar 266-6 cell lines across a concentration

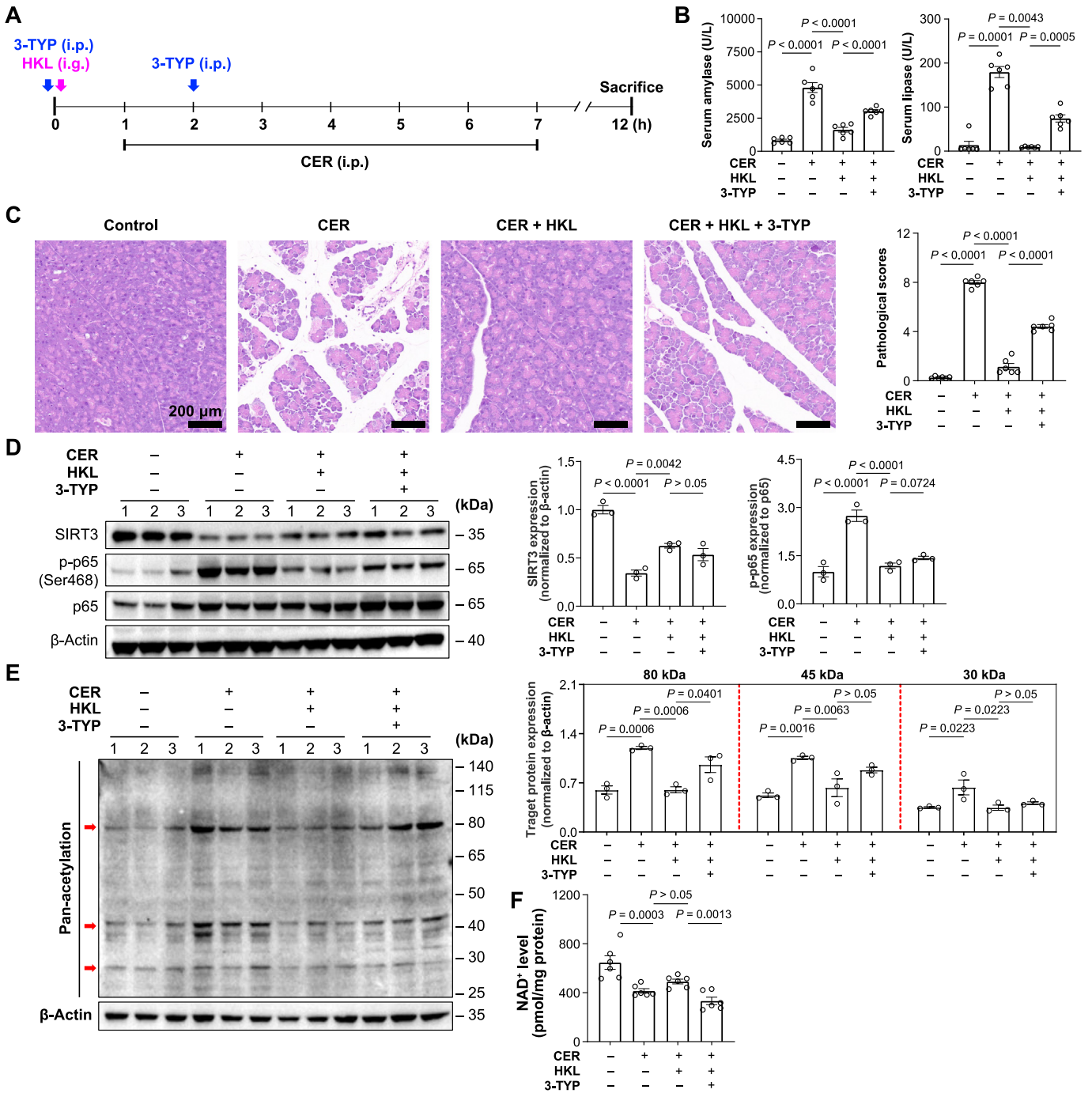

Fig. 3. SIRT3 inhibition reverses the protective effects of HKL in acute pancreatitis. **A:** Schematic illustration of the HKL and 3-TYP rescue experiment design. **B:** Serum amylase and lipase levels (n = 6). **C:** Representative images of pancreatic sections stained with hematoxylin and eosin after HKL treatment with or without 3-TYP co-administration (magnification: 200×) and quantitative analysis of pathological scores (n = 6). **D and E:** Western blot analysis of SIRT3, p65 and p-p65 (D) and pan-acetylated proteins (E) in pancreatic tissues (n = 3). **F:** Quantification of NAD^+ content in pancreatic tissue (n = 6). Data are presented as mean ± standard error of mean. 3-TYP: 3-(1H-1,2,3-triazol-4-yl) pyridine; CER: caerulein; HKL: honokiol; i.g.: intragastric gavage; i.p.: intraperitoneal; NAD^+: nicotinamide adenine dinucleotide (oxidized form); p65: nuclear factor κB p65; p-p65: phosphorylated p65; SIRT3: sirtuin 3.

range of 1.25–80 μmol/L. Honokiol showed no significant impact on cell viability at concentrations up to 10 μmol/L, with mild suppression at 20 μmol/L and marked reductions at 40 and 80 μmol/L (P < 0.01, Fig. 6A). Based on these results, 10 μmol/L was selected as the working concentration of honokiol for subsequent experiments.

caerulein stimulation across a broad concentration range did not significantly affect cell viability in our preliminary experiments, whereas NaT induced dose-dependent cytotoxicity, with cell viability decreasing to 81.79%, 45.44% and 26.64% at 5, 10 and 20 mmol/L, respectively (Fig. 6B); thus, 5 or 10 mmol/L NaT was used to induce the AP model in the subsequent experiments. NaT stimulation also reduced intracellular ATP levels, which were partially restored by honokiol pretreatment (P = 0.0093, Fig. 6C).

Hoechst 33342/PI staining further revealed that honokiol reduced NaT-induced acinar necrosis (Fig. 6D). Consistent with in vivo observations, NaT exposure downregulated SIRT3 and upregulated p-p65 expression, while honokiol pretreatment

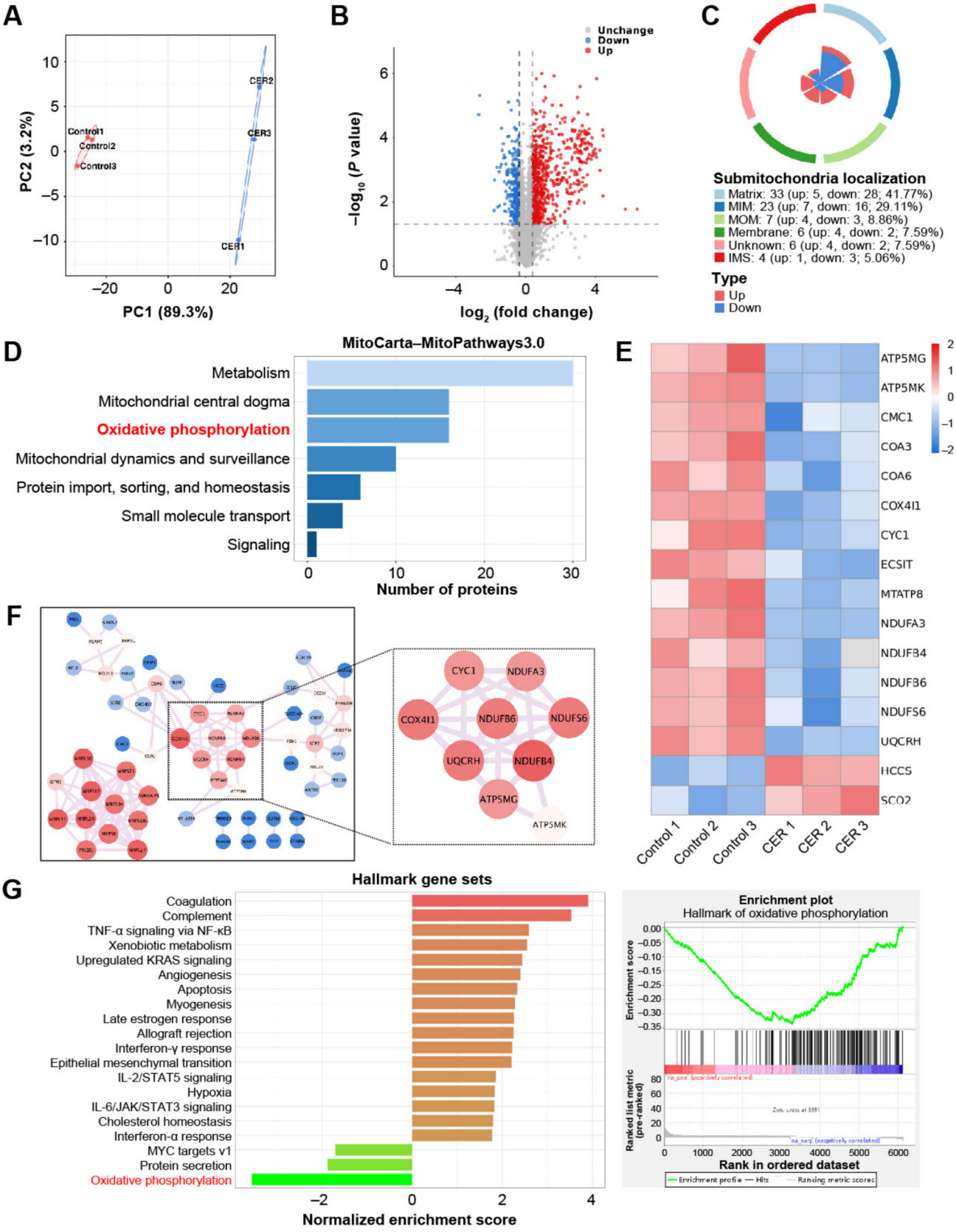

Fig. 4. Proteomic analysis reveals impaired mitochondrial OXPHOS in AP. **A:** Principal component analysis of proteomic profiles in pancreatic tissue samples of control and mice with CER-induced AP. **B:** Volcano plot of DEPs. **C:** Submitochondrial compartment distribution of mitochondrial-associated DEPs based on MitoCarta 3.0 annotations. **D:** Enriched mitochondrial pathways identified using MitoCarta 3.0 pathway analysis. **E:** Heatmap showing the expression of OXPHOS-related proteins (n = 3). **F:** Protein–protein interaction network illustrating clusters associated with mitochondrial gene expression and OXPHOS components, with OXPHOS-related proteins highlighted. **G:** Gene Set Enrichment Analysis of the top 20 enriched biological processes. AP: acute pancreatitis; CER: caerulein; DEPs: differentially expressed proteins; IMS: intermembrane space; MIM: mitochondrial inner membrane; MOM: mitochondrial outer membrane; OXPHOS: oxidative phosphorylation; PC: principal component.

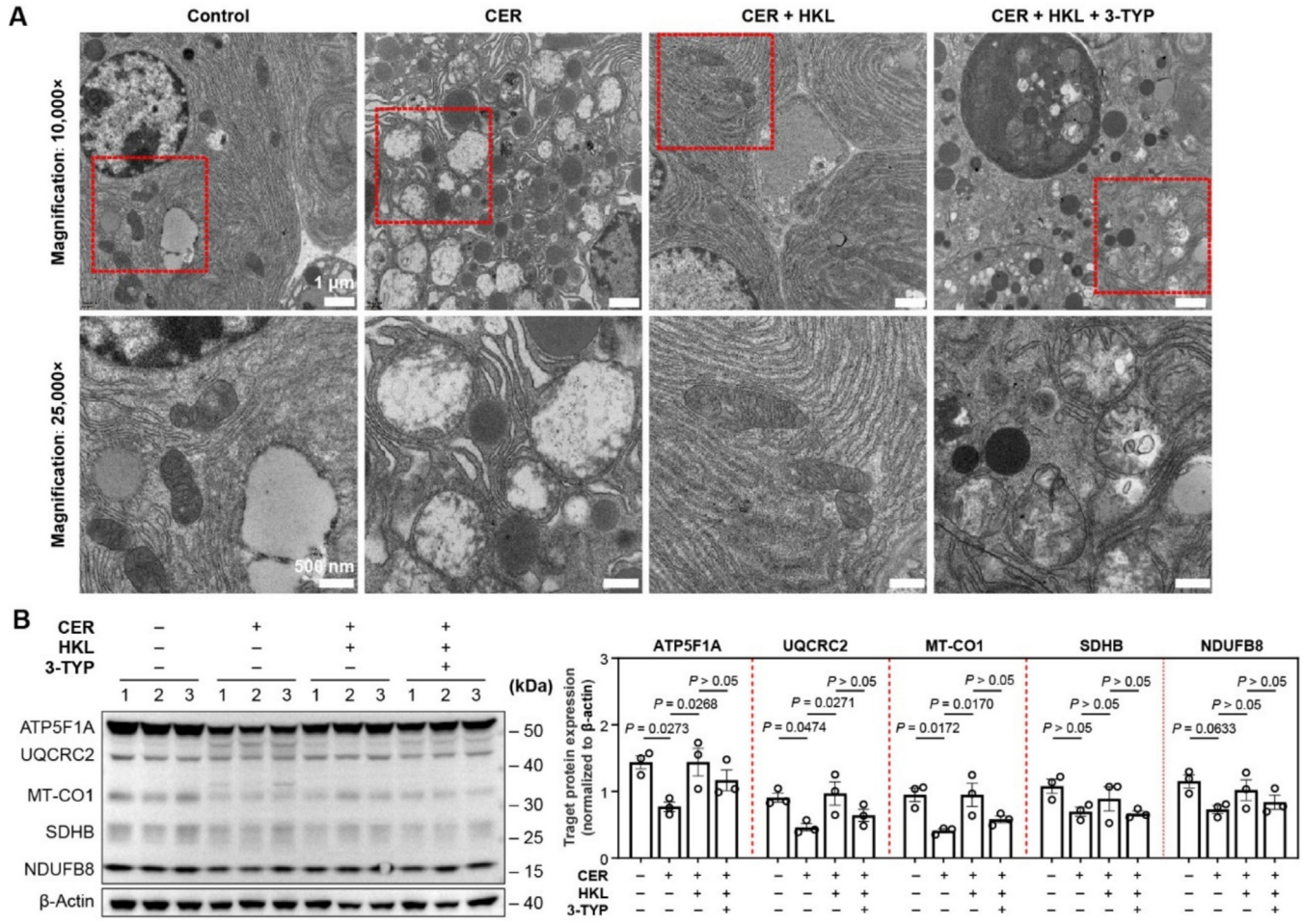

Fig. 5. HKL restores mitochondrial structure and expression of OXPHOS proteins in acute pancreatitis. **A:** Transmission electron microscopy images showing mitochondrial ultrastructure in pancreatic tissue. The lower panel shows magnified views of the areas indicated with red brackets in the upper panel. **B:** Western blotting analysis of OXPHOS complex subunits in pancreatic tissue samples using a rodent-specific antibody cocktail, including ATP5F1A, UQCRC2, MT-CO1, SDHB and NDUFB8 (n = 3). Data are expressed as mean ± standard error of mean. 3-TYP: 3-(1H-1,2,3-triazol-4-yl) pyridine; ATP5F1A: adenosine triphosphate synthase F1 subunit α; CER: caerulein; HKL: honokiol; MT-CO1: mitochondrially encoded cytochrome *c* oxidase I; NDUFB8: NADH:ubiquinone oxidoreductase subunit B8; OXPHOS: oxidative phosphorylation; SDHB: succinate dehydrogenase complex iron sulfur subunit B; UQCRC2: ubiquinol-cytochrome *c* reductase core protein 2.

mitigated these changes (Fig. 6E). Together, these findings indicate that honokiol may mitigate NaT-induced mitochondrial stress and inflammatory signaling in 266-6 cells.

3.7. Honokiol attenuates TLCS-induced injury and inflammatory signaling in PACs

To extend the findings of in vitro studies on the 266-6 cells to a more physiologically relevant model, PACs were isolated and subjected to TLCS stimulation, a well-established method for mimicking acinar injury [31]. Honokiol pretreatment at 5 or 10 μmol/L significantly improved cell necrosis, as assessed by PI staining (both $P < 0.0001$, Fig. 7A). Both concentrations conferred comparable protective effects. Inflammatory cytokine levels measured in the culture supernatant by ELISA revealed that TLCS stimulation markedly increased TNF-α, IL-1β and IL-6 production, which was significantly reduced by honokiol pretreatment (all $P < 0.05$, Fig. 7B). Immunoblot analysis further showed that TLCS upregulated p-p65 levels in PACs, which were attenuated by honokiol at either dose ($P < 0.05$); the reversing effects of honokiol were observed in the TLCS-suppressed SIRT3 expression, however, without statistical significance (Fig. 7C). These results suggest that honokiol protects PACs against TLCS-induced injury, potentially by preserving SIRT3 expression and attenuating NF-κB activation.

3.8. Honokiol promotes SIRT3-mediated deacetylation of CYC1 and alleviates OXPHOS dysfunction in AP

To investigate whether the protective effects of honokiol involve SIRT3-regulated mitochondrial proteins, proteomic analysis was conducted to compare mitochondrial DEPs between AP and honokiol-treated groups. Among these, ATP synthase membrane subunit K (ATP5MK), CYC1 and ubiquinol-cytochrome *c* reductase hinge protein (UQCRH), three key components of the OXPHOS pathway, were downregulated in the caerulein-induced AP model and then partially restored by honokiol treatment (Fig. 8A and 8B). In parallel, NaT stimulation in 266-6 cells led to elevated ROS levels, as indicated by DHE fluorescence. The pretreatment with honokiol markedly reduced ROS accumulation (Fig. 8C), suggesting protection against OXPHOS-related oxidative stress. Protein–protein docking simulations revealed binding energy between SIRT3 and ATP5MK (–27.8 kcal/mol), between SIRT3 and CYC1 (–28.8 kcal/mol) and between SIRT3 and UQCRH (–11.0 kcal/mol), with the SIRT3–CYC1 interaction involving nine predicted binding residues, indicating a particularly strong affinity (Fig. 8D). To further assess whether honokiol enhances SIRT3-mediated deacetylation of CYC1, immunoprecipitation with a pan-acetylation antibody was performed. The level of acetylated CYC1 was elevated but reduced following honokiol treatment in

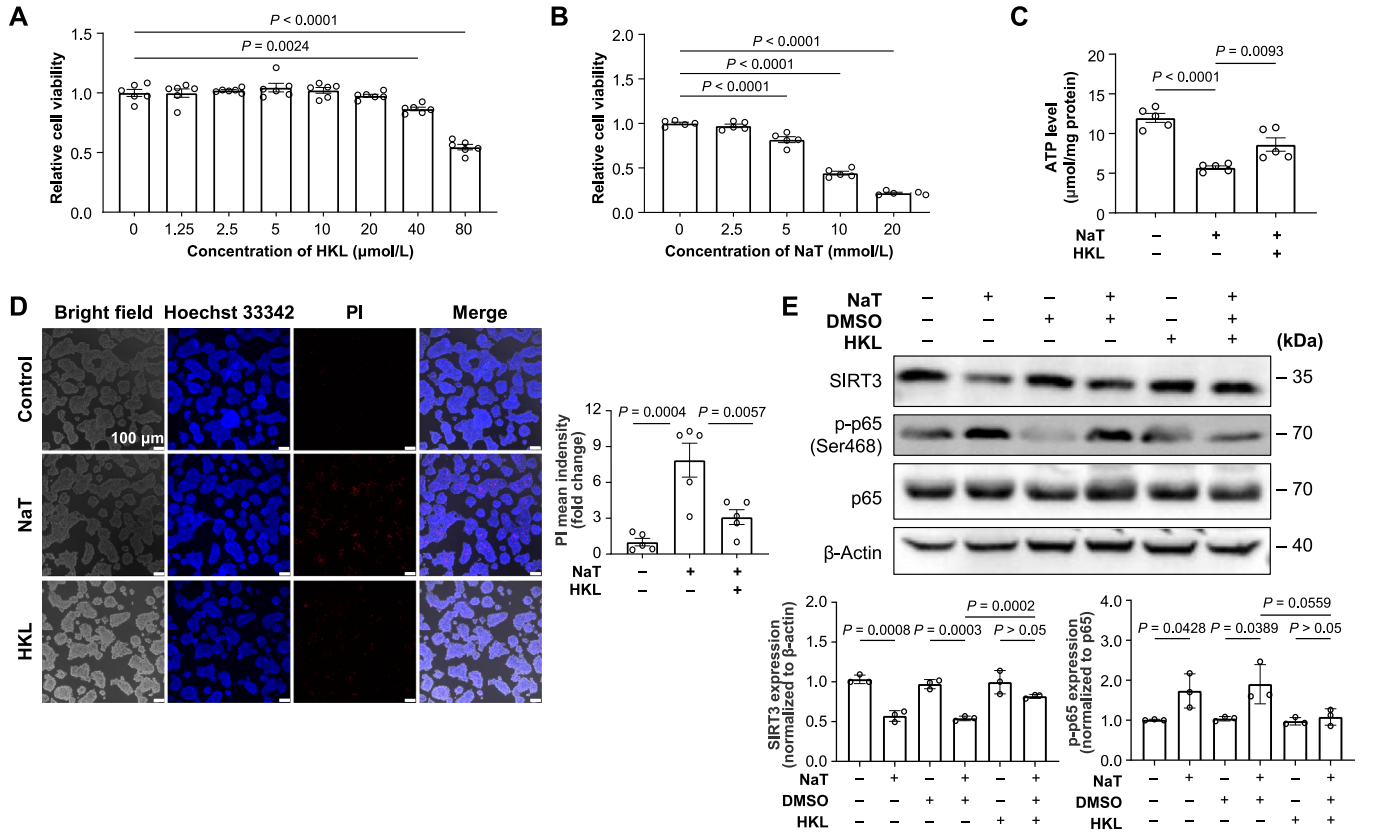

Fig. 6. HKL reduces NaT-induced oxidative stress, necrosis and inflammation in 266-6 cells. **A:** CCK-8 assay evaluating the cytotoxicity of HKL in 266-6 cells (n = 6). **B:** CCK-8 assay assessing the cytotoxicity of NaT in 266-6 cells (n = 5). **C:** Intracellular levels of ATP following NaT exposure (10 mmol/L) and HKL (10 μmol/L) pretreatment (n = 5). **D:** Fluorescence imaging of necrotic cells using Hoechst 33342/PI double-staining in 266-6 cells treated with 10 mmol/L NaT (magnification: 200×) and quantitative analysis (n = 5). **E:** Western blotting analysis of SIRT3, p65 and p-p65 in 266-6 cells treated with 5 mmol/L NaT (n = 3). Data are expressed as mean ± standard error of mean. ATP: adenosine triphosphate; CCK-8: cell counting kit-8; DMSO: dimethyl sulfoxide; HKL: honokiol; NaT: taurocholic acid sodium salt hydrate; p65: nuclear factor-κB p65; p-p65: phosphorylated p65; PI: propidium iodide; SIRT3: sirtuin 3.

AP tissue (Fig. 8E), supporting CYC1 as a downstream target of SIRT3 and a potential regulatory point in honokiol-mediated mitochondrial protection.

4. Discussion

The findings of this study demonstrate a SIRT3-dependent mechanism through which honokiol protects against AP. Temporally, SIRT3 expression was markedly suppressed during AP progression. Pharmacological inhibition of SIRT3 by 3-TYP aggravated pancreatic injury and increased global protein acetylation, underscoring the importance of SIRT3 activity in AP. Proteomic analysis revealed that OXPHOS was the most significantly affected mitochondrial pathway in AP. The administration of honokiol restored SIRT3 expression, mitigated mitochondrial and inflammatory injury, and partially rescued OXPHOS protein levels. Among the OXPHOS-associated candidates, CYC1 was prioritized as a potential SIRT3 target based on protein–protein docking analysis. Immunoprecipitation assays further demonstrated increased acetylation of CYC1 in AP, which was reduced following honokiol treatment, supporting its potential role as a downstream effector of SIRT3 in maintaining mitochondrial integrity.

SIRT3 is widely recognized as a key mitochondrial regulator in various tissues, where its activation improves cellular resilience against oxidative stress, inflammation and metabolic dysfunction [32–34]. However, its role in AP has been relatively underexplored. To date, only three experimental studies have specifically examined SIRT3 in AP. Liu et al. [12] demonstrated that the expression of SIRT3 was markedly downregulated in a caerulein-induced AP model and that its overexpression ameliorated pancreatic injury by reducing oxidative stress and restoring mitochondrial function. Jin et al. [35] reported decreased SIRT3 expression in lung tissue in a severe AP model induced by caerulein and lipopolysaccharide. Another study found that honokiol activated SIRT3 and attenuated hypertriglyceridemia-associated AP in rats; however, the downstream mitochondrial targets were not investigated [13]. Our study was conducted to complement these existing data. We characterized the temporal decline of pancreatic SIRT3 in caerulein-induced AP and showed that pharmacological inhibition of SIRT3 with the selective inhibitor 3-TYP aggravated pancreatic injury and increased global protein acetylation. Given the central role of mitochondria in early acinar cell injury, we subsequently focused on OXPHOS, the core metabolic process that sustains cellular ATP production and redox balance.

Mitochondrial dysfunction, particularly impaired OXPHOS, is a hallmark of early acinar cell injury in AP. Using proteomic profiling combined with annotation via the MitoCarta 3.0 database, our study identified a significant downregulation of OXPHOS-related proteins in AP mice, indicating a disruption in mitochondrial respiratory capacity. These findings align with previous reports showing that mitochondrial collapse leads to ATP depletion, ROS accumulation and necrotic cell death in acinar cells, which triggers inflammatory cascades and further amplifies AP severity [15,36]. In the established AP model in this study, bile acid (NaT/TLCS) stimulation recapitulated these events in vitro, where honokiol pretreatment effectively reversed ATP loss, suppressed ROS generation,

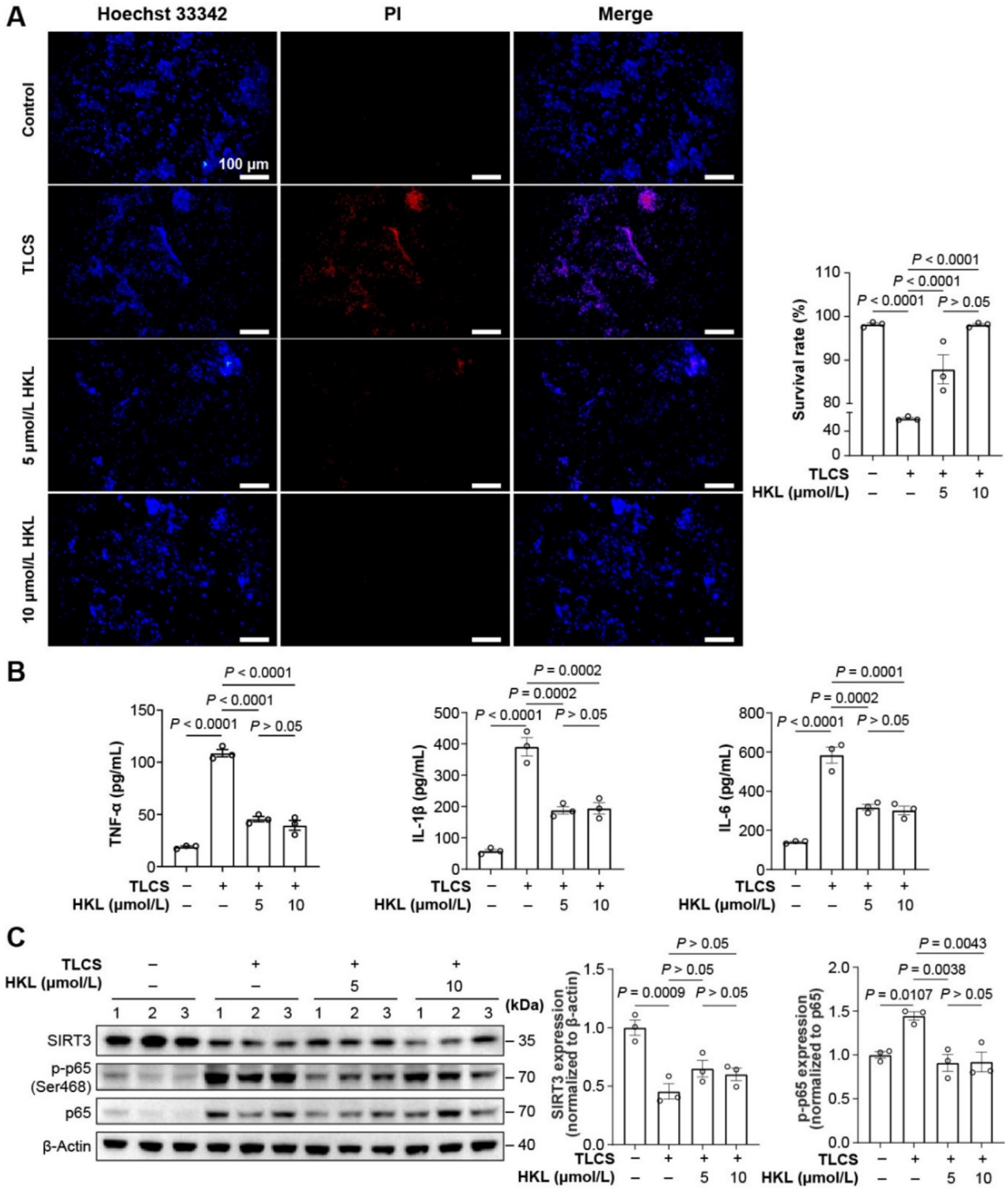

Fig. 7. HKL attenuates TLCS-induced injury and inflammatory signaling in pancreatic acinar cells. **A:** Fluorescence imagesof necrotic cell death using Hoechst 33342/PI staining (magnification: 200×) and quantitative analysis (n = 3). **B:** Enzyme-linked immunosorbent assay of TNF-α, IL-1β and IL-6 in culture supernatants (n = 3). **C:** Western blotting analysis of SIRT3, p65 and p-p65 (n = 3). Data are expressed as mean ± standard error of mean. HKL: honokiol; IL-1β: interleukin-1β; p65: nuclear factor-κB p65; p-p65: phosphorylated p65; PI: propidium iodide; SIRT3: sirtuin 3; TLCS: taurolithocholic acid 3-sulfate disodium salt; TNF-α: tumor necrosis factor-α.

and reduced necrosis and cytokine release, supporting the notion that preservation of OXPHOS function mitigates inflammatory injury.

SIRT3 has been increasingly recognized as a key regulator of mitochondrial function via its NAD^+-dependent deacetylase activity. SIRT3 maintains OXPHOS efficiency by deacetylating specific mitochondrial proteins. For example, in liver mitochondria, SIRT3 deficiency leads to hyperacetylation of ATP synthase subunits and impairs ATP generation [37]; in brown adipose tissue, SIRT3 deletion disrupts lipid oxidation and mitochondrial respiratory chain activity [38]; in heart tissue, SIRT3 deficiency results in hyperacetylation of more than 50 subunits of the electron trans-

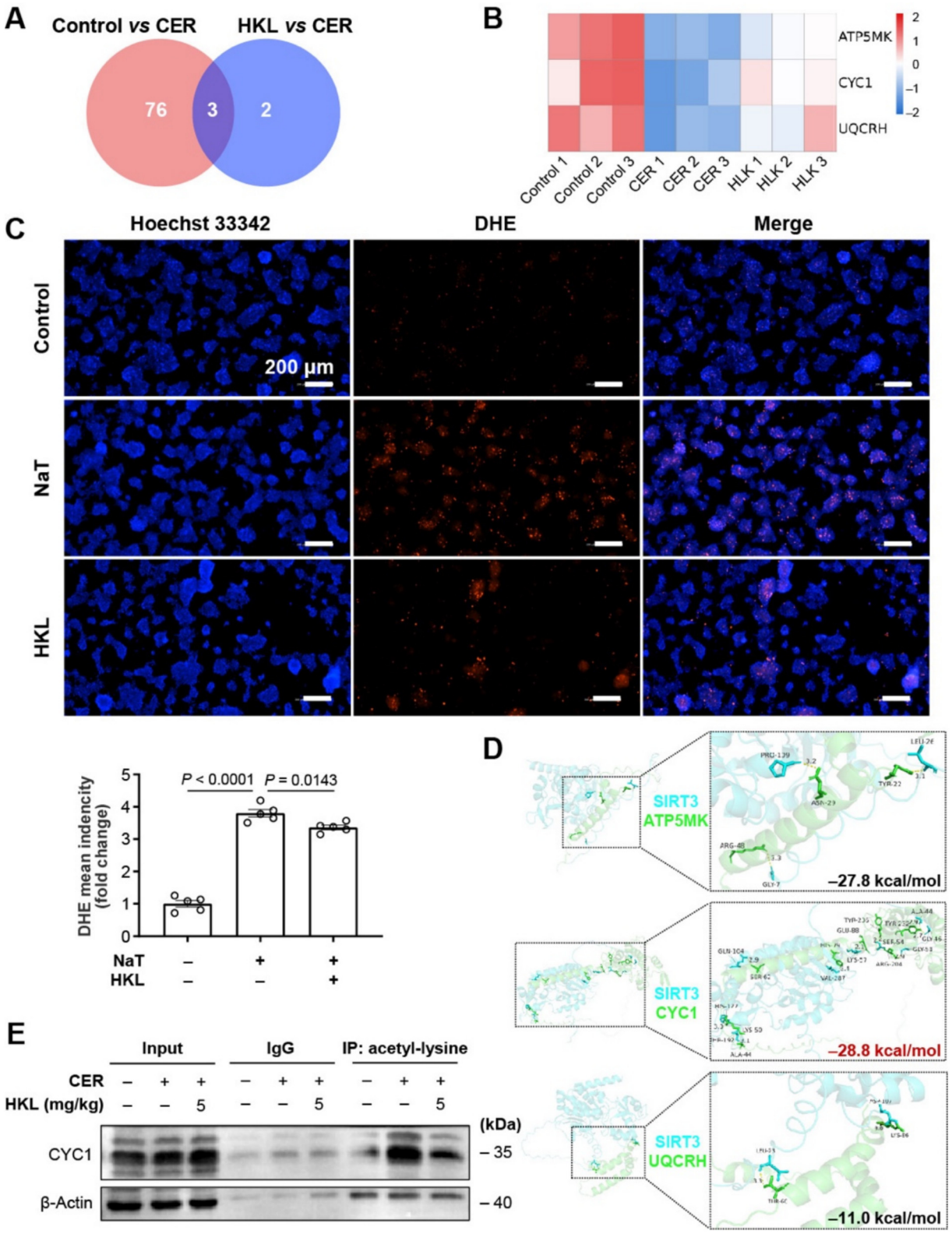

Fig. 8. HKL promotes SIRT3-mediated deacetylation of CYC1 and alleviates OXPHOS dysfunction in acute pancreatitis. **A:** Overlapping differentially expressed proteins of the mitochondria between control *vs* CER and HKL *vs* CER based on proteomic analysis of pancreatic tissues. **B:** Heatmap showing the expression of ATP5MK, CYC1 and UQCRH in pancreatic tissues from control, CER and HKL groups (n = 3). **C:** Fluorescence imaging of reactive oxygen species by DHE staining in 266-6 cells using a Celigo™ imaging cytometer with a 4× objective lens and quantitative analysis (n = 5). **D:** Protein–protein docking simulations of SIRT3 with ATP5MK, CYC1 and UQCRH. **E:** IP analysis of acetylated CYC1 in pancreatic tissues. Data are expressed as mean ± standard error of mean. ATP5MK: adenosine triphosphate synthase membrane subunit K; CER: caerulein; CYC1: cytochrome *c*1; DHE: dihydroethidium; HKL: honokiol; IgG: immunoglobulin G; IP: Immunoprecipitation; NaT: taurocholic acid sodium salt hydrate; OXPHOS: oxidative phosphorylation; SIRT3: sirtuin 3; UQCRH: ubiquinol-cytochrome *c* reductase hinge protein.

port chain, leading to compromised mitochondrial bioenergetics [39]. Collectively, these findings underscore a conserved role of SIRT3 in sustaining mitochondrial respiratory function via lysine deacetylation. Extending this concept to AP, our study suggests that honokiol restores mitochondrial homeostasis by enhancing SIRT3-mediated deacetylation, thereby preserving OXPHOS integrity. As a NAD^+-dependent enzyme, SIRT3 activity is intrinsically tied to NAD^+ availability. In our study, pancreatic NAD^+ levels were significantly decreased in mice with caerulein-induced AP, consistent with findings of a previous study [12]. Honokiol modestly increased NAD^+ content but did not meet the threshold for statistical significance, whereas co-treatment with 3-TYP and honokiol increased the inhibition. These findings suggest a potential feedback loop between NAD^+ availability and SIRT3 function in AP under inflammatory stress. Although honokiol has been reported to restore the NAD^+/NADH ratio in a hepatic encephalopathy model [40], whether it acts through similar mechanisms in AP remains to be investigated.

To explore downstream mediators through which SIRT3 potentially regulates mitochondrial respiration in AP, we performed proteomic analysis and identified that three OXPHOS-related subunits, i.e., ATP5MK, CYC1 and UQCRH, were downregulated in pancreatitis and partially restored by honokiol treatment. Among these, CYC1, a core component of complex Ⅲ that facilitates electron transfer to cytochrome *c*, emerged as a potential SIRT3 target owing to its essential role in maintaining mitochondrial membrane potential and ATP synthesis [41]. To our knowledge, acetylation of CYC1 in mammals has not been previously reported. However, structural studies indicate that lysine acetylation of its interacting partner, cytochrome *c*, impairs electron transfer to complex Ⅳ, thereby attenuating ATP generation [17]. The immunoprecipitation experiments revealed that CYC1 acetylation was markedly increased in AP and reversed by honokiol, supporting the notion that honokiol restores mitochondrial function, at least in part, via SIRT3-mediated deacetylation of CYC1. This finding represents the first evidence that CYC1 acetylation is associated with mitochondrial dysfunction in AP, highlighting a previously unrecognized SIRT3-CYC1-OXPHOS axis that may underlie the therapeutic effects of honokiol on mitochondrial injury in AP.

Nevertheless, this study has several limitations. First, SIRT3 activity was modulated using the administration of 3-TYP, a selective pharmacological inhibitor. Although this approach provides practical advantages, it may not be fully selective for SIRT3, and thus future studies employing genetic models need to be carried out to provide more evidence. Second, while we identified CYC1 as a potential SIRT3 substrate involved in OXPHOS regulation, the specific lysine residues responsible for its acetylation and their functional consequences remain to be identified. Further studies employing immunoprecipitation–mass spectrometry and lysine-mutant constructs are warranted to confirm the mechanistic relevance of CYC1 deacetylation. Moreover, although our findings indicate that NAD^+ depletion may contribute to SIRT3 dysfunction in AP, the upstream regulators of NAD^+ homeostasis and their modulation by honokiol remain to be elucidated. It is believed that understanding how honokiol affects NAD^+ biosynthesis or salvage pathways can provide new therapeutic entry points for mitochondrial protection in AP.

5. Conclusion

Honokiol exerts protective effects in AP by activating SIRT3, enhancing its interaction with CYC1, a core subunit of mitochondrial complex Ⅲ, and promoting its deacetylation. This interaction contributes to the restoration of mitochondrial OXPHOS and mitigation of mitochondrial dysfunction. Collectively, our findings suggest that CYC1 is a novel downstream target of SIRT3 and provide new insight into mitochondrial regulation in pancreatitis.

Funding

This research was supported by National Natural Science Foundation of China (No. 82305076), China Postdoctoral Science Foundation (No. 2023MD744128) and Postdoctoral Science Foundation of Chengdu University of Traditional Chinese Medicine (No. BSH2023004). The funders had no role in the study design or data collection, analysis or interpretation.

Declaration of generative AI and AI-assisted technologies in scientific writing

During the preparation of this work, the authors used ChatGPT by OpenAI to assist with language refinement and phrasing suggestions. After using this tool, the authors reviewed and edited the content as needed and take full responsibility for the content of the publication.

Declaration of competing interest

The authors declare that they have no competing interests.

CRediT authorship contribution statement

YFM: conceptualization, data curation, formal analysis, funding acquisition, investigation, visualization, writing–original draft. **JQY:** data curation, formal analysis, investigation, visualization, writing–original draft. **YP:** formal analysis, investigation, methodology, validation. **DB:** visualization, writing–original draft. **SHF:** validation, visualization. **HYL:** methodology, validation. **WJ:** conceptualization, project administration, writing–review & editing. **YL:** resources, supervision, writing–review & editing.

Acknowledgements

We would like to acknowledge PTM BIO (Hangzhou, Zhejiang Province, China) for the proteomics sequencing services and to extend our special thanks to the regional manager Shuang Zheng for her valuable technical advice throughout the study.

References

[1] Iannuzzi JP, King JA, Leong JH, Quan J, Windsor JW, Tanyingoh D, et al. Global incidence of acute pancreatitis is increasing over time: a systematic review and meta-analysis. Gastroenterology 2022;162(1):122–34.
[2] Schepers NJ, Bakker OJ, Besselink MG, Ahmed Ali U, Bollen TL, Gooszen HG, et al. Impact of characteristics of organ failure and infected necrosis on mortality in necrotising pancreatitis. Gut 2019;68(6):1044–51.
[3] Mederos MA, Reber HA, Girgis MD. Acute pancreatitis: a review. J Am Med Assoc 2021;325(4):382–90.
[4] Szatmary P, Grammatikopoulos T, Cai W, Huang W, Mukherjee R, Halloran C, et al. Acute pancreatitis: diagnosis and treatment. Drugs 2022;82(12):1251–76.
[5] Hey-Hadavi J, Velisetty P, Mhatre S. Trends and recent developments in pharmacotherapy of acute pancreatitis. Postgrad Med 2023;135(4):334–44.
[6] Habtezion A, Gukovskaya AS, Pandol SJ. Acute pancreatitis: a multifaceted set of organelle and cellular interactions. Gastroenterology 2019;156(7):1941–50.
[7] Li J, Chen YF, Gao L, Li YJ, Feng DX. Honokiol prevents intestinal barrier dysfunction in mice with severe acute pancreatitis and inhibits JAK/STAT1 pathway and acetylation of HMGB1. Chin J Integr Med 2024;30(6):534–42.
[8] Ma X, Jin T, Han C, Shi N, Liang G, Wen Y, et al. Aqueous extraction from Dachengqi formula granules reduces the severity of mouse acute pancreatitis via inhibition of pancreatic pro-inflammatory signalling pathways. J Ethnopharmacol 2020;257:112861.
[9] Huang W, Liu H, Li Y, Mai G. The effects of rhein and honokiol on metabolic profiles in a mouse model of acute pancreatitis. Med Sci Monit 2020;26:e925727.

[10] Weng TI, Wu HY, Chen BL, Liu SH. Honokiol attenuates the severity of acute pancreatitis and associated lung injury via acceleration of acinar cell apoptosis. Shock 2012;37(5):478–84.
[11] Pillai VB, Samant S, Sundaresan NR, Raghuraman H, Kim G, Bonner MY, et al. Honokiol blocks and reverses cardiac hypertrophy in mice by activating mitochondrial SIRT3. Nat Commun 2015;6:6656.
[12] Liu LW, Xie Y, Li GQ, Zhang T, Sui YH, Zhao ZJ, et al. Gut microbiota-derived nicotinamide mononucleotide alleviates acute pancreatitis by activating pancreatic SIRT3 signalling. Br J Pharmacol 2023;180(5):647–66.
[13] Meng N, Yang H, Chen J, Qin Y, Lei Y, Huang Z, et al. Honokiol reduces oxidative stress by activating the SIRT3-MnSOD2 pathway to alleviate hypertriglyceridemia-induced acute pancreatitis in rats. Nan Fang Yi Ke Da Xue Xue Bao 2023;43(3):405–11 [Chinese with abstract in English].
[14] Sun L, Leng R, Liu M, Su M, He Q, Zhang Z, et al. Endothelial MICU1 protects against vascular inflammation and atherosclerosis by inhibiting mitochondrial calcium uptake. J Clin Invest 2025;135(7):e181928.
[15] Zhu Q, Yuan C, Dong X, Wang Y, Li B, Tu B, et al. Bile acid metabolomics identifies chenodeoxycholic acid as a therapeutic agent for pancreatic necrosis. Cell Rep Med 2023;4(12):101304.
[16] Rardin MJ, Newman JC, Held JM, Cusack MP, Sorensen DJ, Li B, et al. Label-free quantitative proteomics of the lysine acetylome in mitochondria identifies substrates of SIRT3 in metabolic pathways. Proc Natl Acad Sci U S A 2013;110(16):6601–6.
[17] Márquez I, Pérez-Mejías G, Guerra-Castellano A, Olloqui-Sariego JL, Andreu R, Calvente JJ, et al. Structural and functional insights into lysine acetylation of cytochrome *c* using mimetic point mutants. FEBS Open Bio 2021;11(12):3304–23.
[18] Yao J, Jiang Y, Zhang P, Miao Y, Wu X, Lei H, et al. Genetic and pharmacological targeting of HINT2 promotes OXPHOS to alleviate inflammatory responses and cell necrosis in acute pancreatitis. Pharmacol Res 2025;212:107620.
[19] Lerch MM, Gorelick FS. Models of acute and chronic pancreatitis. Gastroenterology 2013;144(6):1180–93.
[20] Zhai M, Li B, Duan W, Jing L, Zhang B, Zhang M, et al. Melatonin ameliorates myocardial ischemia reperfusion injury through SIRT3-dependent regulation of oxidative stress and apoptosis. J Pineal Res 2017;63(2):e12419.
[21] Schmidt J, Rattner DW, Lewandrowski K, Compton CC, Mandavilli U, Knoefel WT, et al. A better model of acute pancreatitis for evaluating therapy. Ann Surg 1992;215(1):44–56.
[22] Kang F, Xie L, Qin T, Miao Y, Kang Y, Takahashi T, et al. Plasma membrane flipping of syntaxin-2 regulates its inhibitory action on insulin granule exocytosis. Nat Commun 2022;13(1):6512.
[23] Schindelin J, Arganda-Carreras I, Frise E, Kaynig V, Longair M, Pietzsch T, et al. Fiji: an open-source platform for biological-image analysis. Nat Methods 2012;9(7):676–82.
[24] Demichev V, Messner CB, Vernardis SI, Lilley KS, Ralser M. DIA-NN: neural networks and interference correction enable deep proteome coverage in high throughput. Nat Methods 2020;17(1):41–4.
[25] Rath S, Sharma R, Gupta R, Ast T, Chan C, Durham TJ, et al. MitoCarta3.0: an updated mitochondrial proteome now with sub-organelle localization and pathway annotations. Nucleic Acids Res 2021;49(D1):D1541–7.
[26] Shannon P, Markiel A, Ozier O, Baliga NS, Wang JT, Ramage D, et al. Cytoscape: a software environment for integrated models of biomolecular interaction networks. Genome Res 2003;13(11):2498–504.
[27] Subramanian A, Tamayo P, Mootha VK, Mukherjee S, Ebert BL, Gillette MA, et al. Gene set enrichment analysis: a knowledge-based approach for interpreting genome-wide expression profiles. Proc Natl Acad Sci U S A 2005;102(43):15545–50.
[28] Castanza AS, Recla JM, Eby D, Thorvaldsdóttir H, Bult CJ, Mesirov JP. Extending support for mouse data in the Molecular Signatures Database (MSigDB). Nat Methods 2023;20(11):1619–20.
[29] Morris GM, Huey R, Lindstrom W, Sanner MF, Belew RK, Goodsell DS, et al. AutoDock4 and AutoDockTools4: automated docking with selective receptor flexibility. J Comput Chem 2009;30(16):2785–91.
[30] Galli U, Mesenzani O, Coppo C, Sorba G, Canonico PL, Tron GC, et al. Identification of a sirtuin 3 inhibitor that displays selectivity over sirtuins 1 and 2. Eur J Med Chem 2012;55:58–66.
[31] Huang W, Cane MC, Mukherjee R, Szatmary P, Zhang X, Elliott V, et al. Caffeine protects against experimental acute pancreatitis by inhibition of inositol 1,4,5-trisphosphate receptor-mediated Ca^{2+} release. Gut 2017;66(2):301–13.
[32] Peng F, Liao M, Jin W, Liu W, Li Z, Fan Z, et al. 2-APQC, a small-molecule activator of sirtuin-3 (SIRT3), alleviates myocardial hypertrophy and fibrosis by regulating mitochondrial homeostasis. Signal Transduct Target Ther 2024;9(1):133.
[33] Wang D, Cao L, Zhou X, Wang G, Ma Y, Hao X, et al. Mitigation of honokiol on fluoride-induced mitochondrial oxidative stress, mitochondrial dysfunction, and cognitive deficits through activating AMPK/PGC-1α/Sirt3. J Hazard Mater 2022;437:129381.
[34] Hor JH, Santosa MM, Lim VJW, Ho BX, Taylor A, Khong ZJ, et al. ALS motor neurons exhibit hallmark metabolic defects that are rescued by SIRT3 activation. Cell Death Differ 2021;28(4):1379–97.
[35] Jin H, Zhao K, Li J, Xu Z, Liao S, Sun S. Matrine alleviates oxidative stress and ferroptosis in severe acute pancreatitis-induced acute lung injury by activating the UCP2/SIRT3/PGC1α pathway. Int Immunopharmacol 2023;117:109981.
[36] Mukherjee R, Mareninova OA, Odinokova IV, Huang W, Murphy J, Chvanov M, et al. Mechanism of mitochondrial permeability transition pore induction and damage in the pancreas: inhibition prevents acute pancreatitis by protecting production of ATP. Gut 2016;65(8):1333–46.
[37] Vassilopoulos A, Pennington JD, Andresson T, Rees DM, Bosley AD, Fearnley IM, et al. SIRT3 deacetylates ATP synthase F1 complex proteins in response to nutrient- and exercise-induced stress. Antioxid Redox Signal 2014;21(4):551–64.
[38] Sebaa R, Johnson J, Pileggi C, Norgren M, Xuan J, Sai Y, et al. SIRT3 controls brown fat thermogenesis by deacetylation regulation of pathways upstream of UCP1. Mol Metab 2019;25:35–49.
[39] Koentges C, Pfeil K, Schnick T, Wiese S, Dahlbock R, Cimolai MC, et al. SIRT3 deficiency impairs mitochondrial and contractile function in the heart. Basic Res Cardiol 2015;110(4):36.
[40] Anamika TSK. Sirtuin-3 activation by honokiol restores mitochondrial dysfunction in the hippocampus of the hepatic encephalopathy rat model of ammonia neurotoxicity. J Biochem Mol Toxicol 2021;35(5):e22735.
[41] Allen JWA. Cytochrome *c* biogenesis in mitochondria—systems Ⅲ and Ⅳ. FEBS J 2011;278(22):4198–216.